J. Micromech. Microeng. **22** (2012) 113001 (8pp) doi:10.1088/0960-1317/22/11/113001

TOPICAL REVIEW

Three-dimensional silicon micromachining

S Azimi[1,3], J Song[1], Z Y Dang[1], H D Liang[1] and M B H Breese[1,2]

[1] Department of Physics, Centre for Ion Beam Applications (CIBA), National University of Singapore, 117542, Singapore
[2] Singapore Synchrotron Light Source (SSLS), 5 Research Link, National University of Singapore, 5 Research Link, 117603, Singapore

E-mail: g0800837@nus.edu.sg

Received 8 June 2012, in final form 2 August 2012
Published 25 September 2012
Online at stacks.iop.org/JMM/22/113001

Abstract
A process for fabricating arbitrary-shaped, two- and three-dimensional silicon and porous silicon components has been developed, based on high-energy ion irradiation, such as 250 keV to 1 MeV protons and helium. Irradiation alters the hole current flow during subsequent electrochemical anodization, allowing the anodization rate to be slowed or stopped for low/high fluences. For moderate fluences the anodization rate is selectively stopped only at depths corresponding to the high defect density at the end of ion range, allowing true three-dimensional silicon machining. The use of this process in fields including optics, photonics, holography and nanoscale depth machining is reviewed.

(Some figures may appear in colour only in the online journal)

1. Introduction

Silicon machining may be defined as the ability to produce patterned structures on or beneath the wafer surface [1], allowing the fabrication of components which are important in many fields like micro/nano-electro-mechanical systems (M/NEMS) [2], silicon photonics [3], microelectronics [4, 5], biology [6], etc. Fabricating such micro- and nano-scale structures such as wires, waveguides, bridges or cantilevers is an important constituent component for these research fields and much effort has been devoted for device design, fabrication and integration for developing future micro/nanotechnologies.

Fabricating complex, arbitrary-shaped silicon structures in three dimensions (3D) is of great importance for different mechanical, electronic and optical devices. Various techniques have been described in the literature for 3D silicon micro/nanofabrication. Surface machining which uses deposited thin films or SOI wafers may be used [7, 8]. The top layer is selectively etched using mask patterns; then the sacrificial layer is removed, producing free-standing silicon structures. This approach uses SOI (silicon-on-insulator) wafers which makes it expensive, or depositing polysilicon layers which results in non-crystalline silicon structures. The cavity-SOI (CSOI) technique uses a thin wafer bonded with another wafer having pre-etched cavities for making free-standing structures on bulk silicon. The 3D structures are etched in the thinned device layer above the cavities located in the handle wafer [9]. Focused ion beams (FIB) [10, 11] are used for silicon surface milling by scanning the beam over the sample to etch arbitrary shape patterns. 3D fabrication is possible using a FIB combined with other methods [12, 13]. Both surface machining and FIB techniques are unable to fabricate 3D structures within the bulk of the wafer. The most common method for bulk silicon micro/nano-machining is deep reactive ion etching (DRIE) [14], used for making structures with vertical sidewalls [15]. However, it is limited in fabricating complex 3D structures. Other techniques such as grey scale, multiple lithography, or controlling the degree of under-etching can help to make curved silicon structures [16–19]. For fabricating free-standing structures on bulk silicon using DRIE, SOI wafers [20] or CSOI technology

[3] Author to whom any correspondence should be addressed.

 © 2012 IOP Publishing Ltd Printed in the UK & the USA

[9] may be used, introducing additional flexibility. Making more complex structures, such as arbitrary free-standing 3D structures at certain depths or multilevel structures in bulk silicon are highly challenging using standard fabrication processes.

The process described in this review using high-energy ion beam irradiation is unique in fabricating complex 3D structures in a direct and flexible way in bulk silicon. In the 1970s nuclear microprobes were developed to focus high momentum MeV ion beams. They are typically based on the use of quadrupole lens multiplets [21, 22], which provide a much stronger focusing action than axially symmetric lenses. Microprobes were mainly used for microanalysis using a range of ion beam techniques but more recently their use for direct writing and patterning of polymer resists for a range of applications was developed [23]; in this same review the use of ion irradiation to selectively control the wavelength of photoluminescence emitted from porous silicon (PSi) was described so this is not discussed further here.

The fabrication process is based on the defects created by high-energy ions in crystalline materials, at the surface and along their trajectory [24–28]. The defect density in silicon due to ion irradiation depends on many factors; defects can be stable or they may agglomerate into more stable divacancies and other vacancy or impurity-related centres. Many types of defects act as trap levels where charge carriers undergo recombination, so reducing the hole density and increasing the resistivity along the ion trajectories. Ion irradiation thus reduces the electrical hole current flowing through these regions during subsequent electrochemical anodization, slowing down or completely stopping the formation of PSi. This process uses p-type silicon within a range of resistivity from $\rho \sim 0.01\ \Omega$ cm (doping density $\sim 10^{19}$ cm^{-3}) to 1 Ω cm (doping density $\sim 2 \times 10^{16}$ cm^{-3}). The lower resistivity wafers are ideal for machining different surface topographies, such as patterned Bragg reflectors, concave micromirrors and holographic surfaces, since the etch rate is proportional to the fluence. Higher resistivity wafers are more suitable in silicon photonics where the lower doping density gives lower scattering losses from free carriers. While a similar process has been used to machine III–V semiconductors such as [29, 30], here we focus on machining and patterning of silicon.

2. Modes of ion irradiation

The use of a microprobe to provide a small MeV ion beam spot which is then scanned over a small sample area is well established, and used for microanalysis and also for direct beam writing (also called proton beam writing). It is very flexible, enabling high spatial resolution and direct fluences to be used in the same area. It does however suffer from the usual problems of all direct write processes, such as limited scan size (typically 1 mm), small throughput owing to the low beam current (typically a few pA) and non-uniform irradiated areas if the beam current fluctuates.

A simple modification to the standard operation of a nuclear microprobe provides a means of solving these problems, allowing rapid irradiation of large wafer areas with

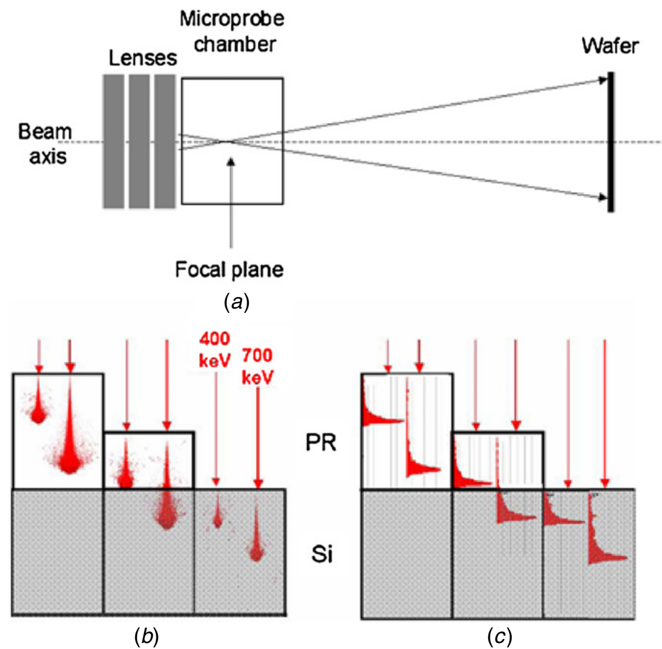

Figure 1. (*a*) Schematic of a large area irradiation system based on a nuclear microprobe quadrupole multiplet focusing system. ((*b*), (*c*)) SRIM plots of 400 and 700 keV H_2^+ ions incident on different thicknesses of photoresist (PR) on top of a 7 μm thick Si layer (shown in grey). From left to right the PR thicknesses are 7 μm, 3 μm and 0. (*b*) Trajectory plots showing how far each ion penetrates through the layer structure. (*c*) Corresponding defect density. Both beam energies are shown with the higher energy to the right. Reprinted with permission from [31]. Copyright 2008, the Optical Society of America.

MeV ions [31]. Figure 1 shows a schematic of a standard microprobe lens multiplet focusing the beam in the chamber, as in normal operation. For large area operation, the collimator and object apertures are opened wide to give a focused beam current of several hundred nanoamperes within the microprobe chamber. The wafer is positioned downstream of the chamber where the highly divergent beam exiting the quadrupole multiplet is uniformly distributed over a large area. For example, locating the sample about 50 cm downstream allows an irradiated area of more than 25 $\times$ 25 mm^2. A MeV helium ion beam current of 500 nA delivers fluences of $\sim 10^{14}$ cm^{-2}, typical of those required to form many micromachined components in a few minutes. A further beneficial aspect of this irradiation mode is that the irradiated beam uniformity is excellent, since any change in beam current equally affects the whole irradiated area.

Patterned irradiation is achieved using a standard ultraviolet photolithography to first deposit a resist layer of a few micrometres in which a certain ion energy is stopped, so that only the exposed wafer areas are irradiated. More complex photoresist patterns can be used in conjunction with multiple energy irradiation to achieve multilevel wafer patterning. Figure 1(*b*) shows SRIM (stopping and range of ions in matter) [26] plots of two ion energies incident on different photoresist thicknesses. By suitable choice of layer thicknesses and beam energies, the defect depth distribution can be located at any wafer depth, allowing the etching rate to be defined laterally and in depth.

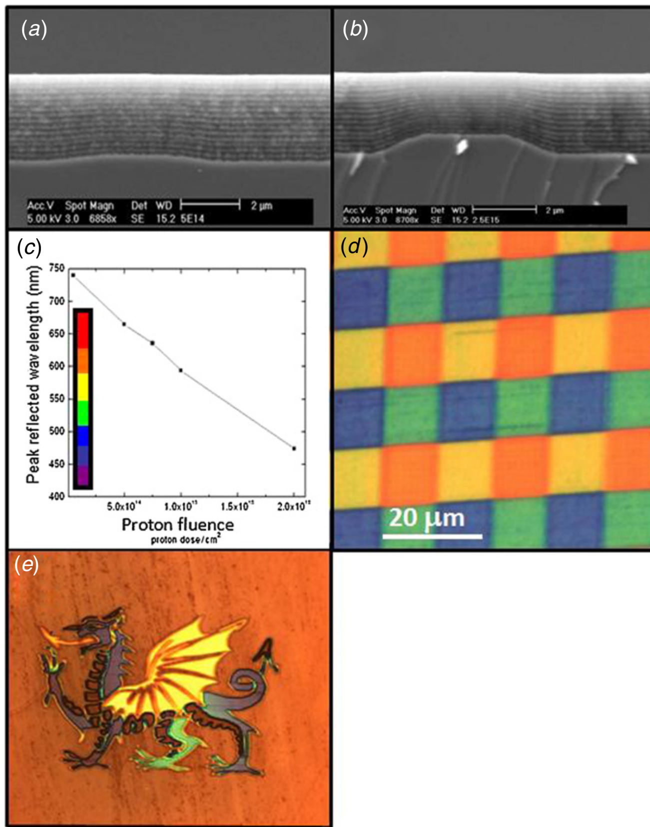

Figure 2. ((*a*), (*b*)) DBRs formed across a 4 μm wide region irradiated 2 MeV proton fluence of 5×10^{14} cm^{-2} and 2.5×10^{15} cm^{-2}, respectively, etched with an alternating current density of 10 and 100 mA cm^{-2} for 4 s each layer, for 15 periods. (*c*) Change in the peak reflected wavelength of irradiated DBR versus proton fluence. (*d*) Patterned DBR formed by irradiating groups of four 10 μm wide pixels with different proton fluences prior to anodization. (*e*) Dragon patterned DBR structure. (*a*), (*b*) and (*d*) reprinted with permission from [32]. Copyright 2006, American Institute of Physics. (*c*) Reprinted with permission from [62]. Copyright 2007, Optical Society of America. (*e*) Reprinted with permission from [37]. Copyright 2007, Elsevier.

3. Surface patterning of low resistivity p-type wafers

Figures 2(*a*) and (*b*) show cross-sectional SEMs of a low resistivity (0.02 Ω cm) p-type wafer irradiated with different fluences of 2 MeV protons along a 4 μm wide line [32]. A progressive height difference between the underlying irradiated surface and that of the unirradiated background is observed, owing to a reduction in the etch current at irradiated areas due to a reduced anodization rate with fluence. This behaviour is used to fabricate a range of different components in low resistivity wafers, utilizing the different properties of the irradiated and unirradiated PSi or the underlying silicon surface relief pattern.

3.1. Distributed Bragg reflectors

The ability to alter the porosity/refractive index of PSi in a periodic manner by alternately raising and lowering the etch current density during anodization is used to produce distributed Bragg reflectors, in which each layer is a quarter of the optical thickness of one incident wavelength [33, 34]. By sandwiching a half wavelength PSi layer between two such DBRs, a resonant cavity is formed which can narrow and enhance the PL emitted [35]. Low resistivity (0.001–0.1 Ω cm) p-type wafers are typically used for this as a greater range of refractive index can be produced by changing the anodization current density [36].

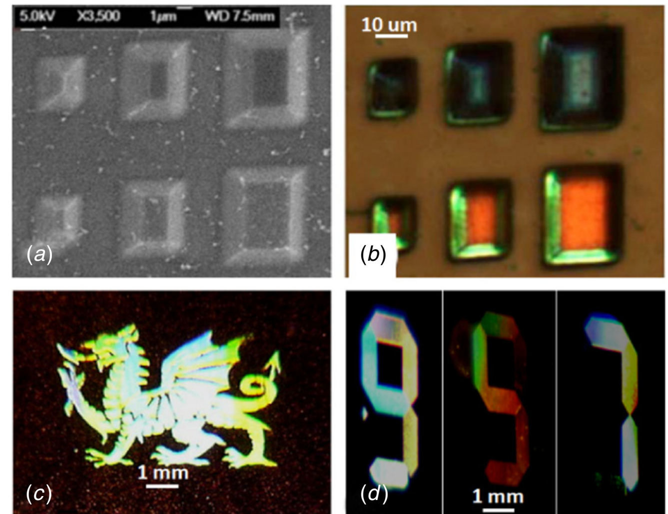

Figure 3. 3D patterned DBR arrays: (*a*) SEM, (*b*) high magnification optical micrograph showing the effect of white light illumination from the top and from the left sides of such pixels. ((*c*), (*d*)) Low magnification optical micrograph of large area arrays of patterned 3D DBR pixels. Reprinted with permission from [37]. Copyright 2008, American Institute of Physics.

Patterned irradiation with MeV ions introduces an extra flexibility into DBR fabrication by allowing selectively irradiated areas to have different reflective wavelengths, owing to the reduced etch current flowing after irradiation. In figures 2(*a*) and (*b*), the reduction in anodization current at irradiated regions results in thinner layers in the PSi DBR. Figure 2(*c*) shows a linear relationship between the DBR reflected wavelength and fluence, allowing local tuning of the reflected wavelengths. Figure 2(*d*) shows an example of the patterned DBR with 10 μm square pixels. Figure 2(*e*) and (*f*) show more complex examples of patterned DBRs made with direct writing. When the large area irradiation facility described above is used, it allows patterned DBRs with micrometre resolution over large areas.

From figures 2(*a*) and (*b*), irradiation not only produces a region where etching is slower and therefore thinner layers in the DBR, but also the zone between the unirradiated and irradiated regions becomes progressively more tilted with fluence. This feature is used to produce arrays of 3D DBR pixels with tunable tilt-angles of the boundary regions, allowing different reflected wavelengths from the sides as well as the tops of the pixels [38]. Figure 3(*a*) shows an array of such pixels where the top, flat surface and tilted sides are seen. Figure 3(*b*) shows the effect of white light illumination from the top and from the left side. A higher fluence is used in fabricating the upper row than the lower row, resulting in the central reflected wavelength from the tops of the upper row pixels being more blue-shifted. Suitable

side illumination produces red-shifted reflected light from the lower pixel boundary compared to the top surface, owing to the longer path length through the tilted DBR. Figures 3(*c*) and (*d*) show examples of patterned DBRs, comprising arrays of pixels, each of which is fabricated utilizing the controlled tilt angle of an etched boundary. This enables 'white' DBRs to be produced by inducing a change in layer thickness at a boundary with etch depth, leading to a wide range of reflected wavelengths, figure 3(*c*). This process also enables patterned areas of DBRs showing different patterns at different tilts or with different angles of illuminated light, figure 3(*d*).

3.2. Surface machining of small surface steps

The same irradiation and anodization process is used for fabricating silicon surface relief structures in low resistivity wafers, such as single/multiple step heights, concave surfaces or free-standing films and structures. It only requires the additional final step of removing the etched PSi, typically using dilute potassium hydroxide (KOH) [39–41]. Different ion fluences may be used to machine silicon surfaces with precisely controlled heights, and a high fluence may completely stop the etching at the irradiated regions [39]. The relationship between irradiation fluence and reduced PSi formation rate follows that shown in figure 2(*c*), and using this method the 'checkerboard' silicon surface pattern shown in figure 4(*a*) was fabricated by irradiating two sets of orthogonal bars with different fluences using direct writing [39].

While in this case, steps up to several micrometres are produced, by carefully controlling the fluence and anodization depth, step heights of only hundreds or tens of nanometres can be similarly machined. This can be done using either direct writing or a patterned photoresist in conjunction with large area irradiation to fabricate multi-step height patterns with low roughness due to the highly uniform fluence. Figure 4(*b*) shows such an example of a range of step heights produced in this way. The silicon surface looks rough, largely because of small pieces of PSi sticking to the surface which are not easily removed. To remove all remaining traces of PSi and further smoothen the silicon surface, thermal oxidation is used [42, 43], after which the same surface in figure 4(*c*) is much smoother. Figure 4(*d*) shows a single step of less than 20 nm, fabricated using a similar process.

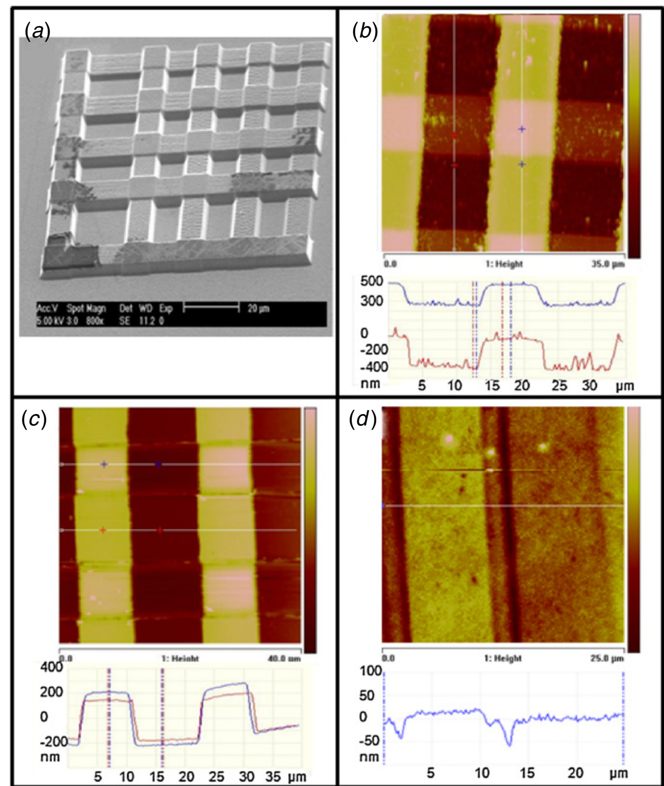

Figure 4. (*a*) SEM image of checkerboard silicon surface pattern having many different heights. Fabricated with irradiating two sets of crossing bars, each with fluences of 2, 4, 6, 8 and 10×10^{15} protons cm^{-2} using 2 MeV protons. ((*b*), (*c*)) AFM images and line scans of surface relief pattern of 10 μm squares of four different heights, created using large area irradiation with 1 MeV proton fluences in orthogonal directions of 1 and 1.1×10^{15} protons cm^{-2}. (*d*) AFM line profile across adjacent 10 μm wide bars showing a 20 nm step height. (*a*) Reprinted with permission from [39]. Copyright 2010 American Institute of Physics.

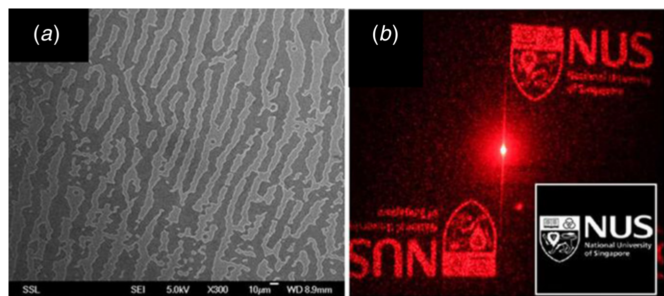

Figure 5. (*a*) SEM image of transferred binary amplitude CGH pattern in silicon irradiated with 600 keV helium ions at 5×10^{14} ions cm^{-2}. (*b*) show grey-scale reconstructed holograms from binary amplitude CGH on silicon. Reprinted with permission from [40]. Copyright 2010 Elsevier.

3.3. Computer-generated holography

Computer-generated holograms (CGH) are used as diffractive-optical elements for storage of digital data and images [44], precise interferometric measurements [45], pattern recognition [46], data encryption [47] and three-dimensional displays [48]. They are described mathematically by computing the phase and amplitude information of the wave propagation produced by an object, rather than physically recording it. A binary surface relief CGH pattern may be machined in silicon [40] by patterning using photolithography with suitable computed patterns, and then irradiating over a large area. After anodization and removing the PSi layer, a binary surface relief CGH pattern is revealed, figure 5(*a*). Figures 5(*b*), (*c*) and (*d*) show examples of reconstructed images from such CGH patterns on silicon by reflecting a red (650 nm) laser off the CGH pattern onto a viewing screen. It is hard to record CGH patterns with variable pixel modulation of both amplitude and phase, so existing recording techniques generally modulate in an on/off binary manner, as in figure 5. Since our micromachining process can variably modulate the

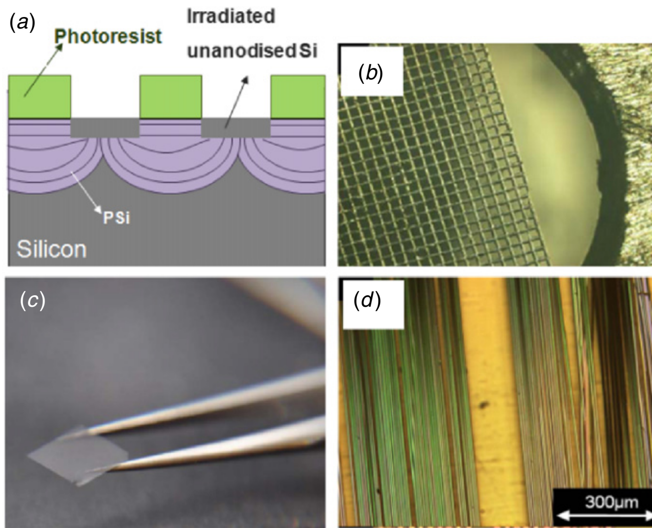

Figure 6. (*a*) Schematic of producing undercut, detached silicon microstructures, where the PSi etch front undercuts the irradiated regions, forming curved surfaces. ((*b*), (*c*)) Free-standing silicon grid fabricated over a 5 × 5 mm^2 area using this process. (*d*) Optical micrograph of many 3.5 μm thick, 5 μm wide silicon bars.

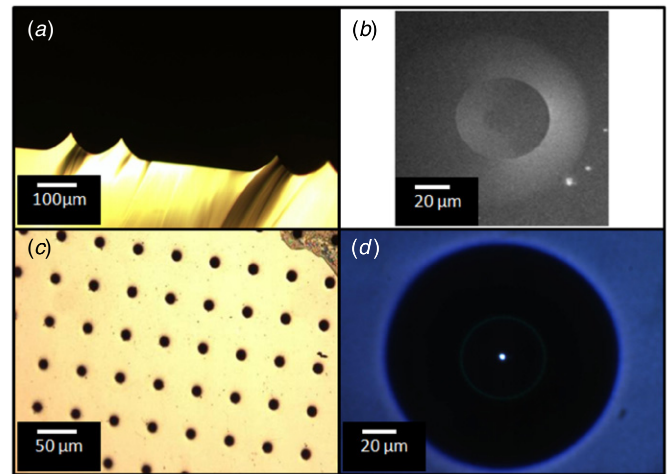

Figure 7. (*a*), (*b*) Optical and SEM images of concave silicon surfaces, (*c*) optical image of an array of concave surfaces with 20 μm diameter. (*d*) Optical image of a concave DBR mirror illuminated with white light, reflecting and focusing blue wavelengths. Reprinted with permission from [41]. Copyright 2010, Optical Society of America.

amplitude of reflected light over a wide range by controlling the surface roughness [49], it may provide a means of modulating both reflected light intensity and phase.

3.4. Free-standing structures

By extending the above process, free-standing silicon structures can be fabricated simply by continued anodization which results in completely undercut irradiated structures. The wafer is first patterned with a photoresist with the inverse pattern of the desired free-standing structure, and then irradiated with a high ion fluence to completely stop PSi formation during subsequent anodization. Thus, PSi forms only at unirradiated regions, figure 6(*a*), and after etching beyond the ion penetration depth, the irradiated regions become undercut. Once they are fully undercut, the surrounding PSi is removed to detach the structure from the silicon substrate. The thickness of the free-standing structure is thus controlled by the ion end-of-range depth, which depends on the ion type and energy. Figures 6(*b*) and (*c*) show a free-standing 3.5 μm thick silicon grid fabricated using 600 keV helium ions. Figure 6(*d*) shows an optical micrograph of many 3.5 μm thick, 5 μm wide bars produced in this same manner, resting on the underlying silicon surface, though completely detached from it.

3.5. Micromirrors—spherical surface patterning

A concave surface profile with micrometre-scale dimensions is of interest because of its ability to focus incoming light into a spot. Concave mirrors act like optical tweezers to trap/push particles with the optical gradient/scattering force [50, 51] and may be used as a variable optical attenuator [52] or to produce an enhanced and localized light signal for parallel low loss optical interconnect systems [53].

We have fabricated very smooth, concave mirrors [41] using ion irradiation of a resist patterned as an annulus, using the same process to produce undercut structures as shown in figure 6(*a*). However, here we make use of the surface relief pattern formed on the underlying silicon substrate after anodization and PSi removal. Ion irradiation creates defects only in the exposed annuli, and so during anodization PSi only forms at the surface within the small central aperture. Since PSi formation is isotropic, a curved etch front naturally forms after the top irradiated region is undercut. A large electropolishing pulse at the end of the anodization detaches the PSi layer and the undercut, patterned structure from the underlying concave silicon surface. The location, diameter and height of the concave surfaces are controlled by the photoresist geometry. Figures 7(*a*) and (*b*) show an optical micrograph and an SEM image of a concave spherical mirror fabricated using this method. An array of such concave mirrors is demonstrated in figure 7(*c*). They can similarly be fabricated with a DBR at the surface, giving the ability to selectively reflect and focus particular wavelengths. A concave surface is first produced, and then the PSi removed, followed by a second anodization step using an alternate high/low current density to achieve a thickness corresponding to one quarter of the desired wavelength. Figure 7(*d*) shows an optical image of one such mirror illuminated with white light, designed to focus and reflect blue light.

4. Three-dimensional patterning in moderate resistivity wafers

There are many fields of science and technology where precisely machined, 3D micro-scale structures are required in silicon-based materials. For example, in silicon photonics conventional silicon waveguide structures are fabricated in SOI wafers, which do not readily allow 3D waveguides between circuitry at different depths within the wafer. Therefore the

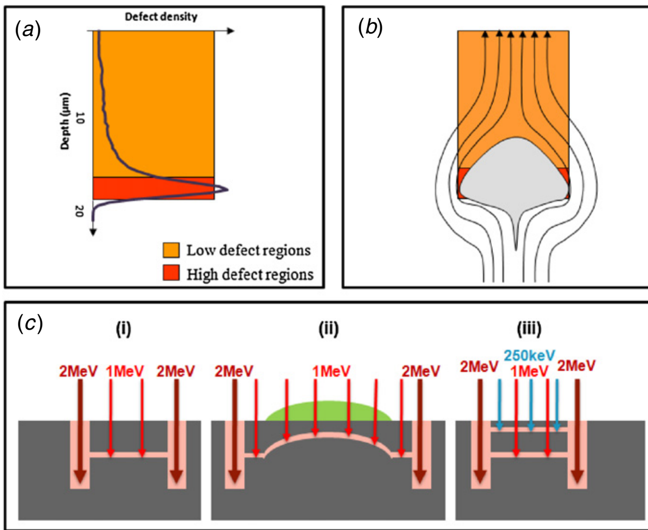

Figure 8. (*a*) Schematic of defect density versus depth for 1 MeV protons in silicon. (*b*) Schematic showing hole current deflected around end-of-range regions owing to their higher defect density. (*c*) Schematic of fabricating (i) flat, (ii) curved and (iii) multilevel free-standing 3D structures. Higher energy ions and high fluences used to completely stop anodization at irradiated regions are used to form supporting walls.

ability to controllably fabricate 3D lines and wires is highly desirable for coupling between circuits at different depths and allowing better 3D integration and packing density of photonic devices with each other and with microelectronic components. It would also allow new options for the design and fabrication of high-aspect ratio, multilevel microstructures in silicon for optoelectronic and in micro-electromechanical systems and in fabricating photonic crystals [54].

A variety of complex shapes, curved or multilevel silicon wires and structures can be fabricated with our process, making use of the fact that for high-energy protons the defect generation rate is more than ten times higher at the end-of-range compared to the trajectory closer to the surface [55]. By controlling moderate fluences within each point of an irradiated area, the resistivity can be increased locally [56] at the end-of-range, figure 8(*a*). During subsequent etching the flow of electrical holes from the back surface bends around the high defect regions to the front surface. As a result PSi forms around these regions, leaving the core region intact, with a size and depth depending on the proton fluence and energy, figure 8(*b*). Figure 8(*c*) shows a schematic of different types of 3D free-standing structures which can be fabricated using this approach.

Figures 9(*a*) and (*b*) show examples of long, free-standing lines and curved lines created using 1 MeV protons to produce end-of-range core regions at a depth of 15 μm, beneath the silicon surface. After etching beyond the core depth, free-standing wires were released by removing the PSi. Microstructures curved in the vertical plane can be similarly micromachined, with the addition of a thin, patterned grey-scale resist mask with tapered edges, figure 8(*c*), part (ii). The resist is thin enough, so that protons can penetrate the underlying silicon. Because of the resist thickness, the proton end-of-range depth in the silicon is modified according to the resist profile. Such spatial variations of the end-of-range enable 3D silicon microstructures which are curved in the vertical direction, see figures 9(*c*) and (*d*).

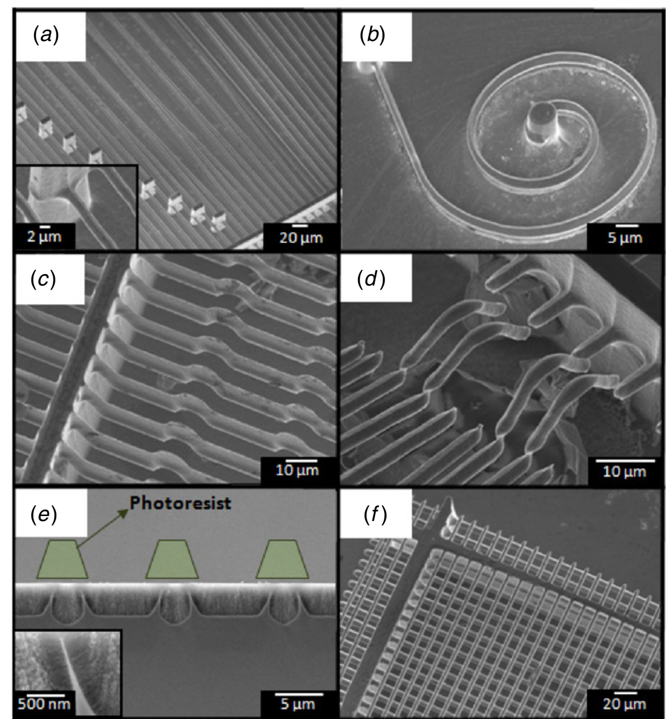

Figure 9. SEM images showing examples of each process in figure 8(*c*). (*a*) and (*b*) show examples of process (i), with 1 MeV proton irradiation with a low line fluence of 1×10^{10} cm^{-1} used to create end-of-range cores and 2 MeV protons with a high line fluence of 1.2×10^{12} cm^{-1} used to create supporting walls for 3D free-standing structures. (*c*) and (*d*) show examples of curved 3D fabrication using process (ii). (*e*) 3D line structure irradiated with a fluence of 1×10^{15} cm^{-2} in 0.01 Ω cm silicon wafer. Green trapeziums indicate the locations of the photoresist during irradiation. (Reprinted with permission from [57] Copyright 2011, The Electrochemical Society). (*f*) Multi-level grids created using process (iii).

Similarly, patterned photoresists with sloping sidewalls may be used to vary the proton end-of-range laterally to fabricate silicon lines with nano-sized tips [57], figure 9(*e*). The flat top of the photoresist is thick enough to completely stop the incoming ions from reaching the underlying silicon. However, ions are able to penetrate the photoresist thinner sloping sidewalls to reach the silicon beneath, producing sloping silicon lines following the photoresist profile. Multiple energy proton irradiation can be used to create localized defect cores at different depths within the silicon wafer to fabricate multilevel 3D structures, figure 8(*c*), part (iii). Figure 9(*f*) shows two-level silicon wire arrays fabricated using this method.

4.1. Waveguides for silicon photonics

Several different types of silicon waveguides have been fabricated in 1–10 W cm p-type silicon using the approach described above, either with direct writing [58] or large area irradiation. Figure 10(*a*) shows silicon-on-oxidized-porous-silicon (SOPS) strip waveguides with high-index contrast

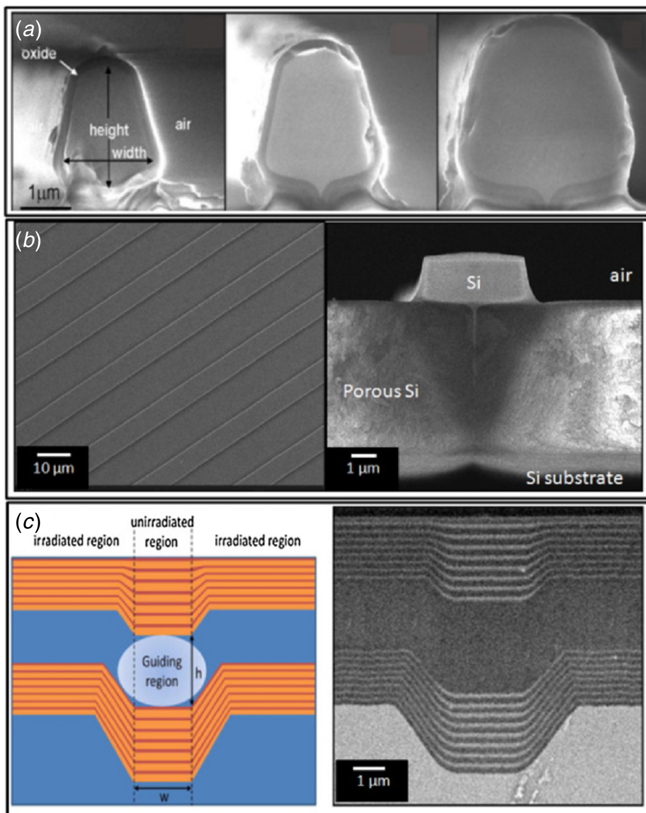

Figure 10. SEM images of SOPS strip waveguides (*a*) direct-write irradiated with 250 keV protons fluences of 7 × 10^{13}, 1 × 10^{14}, 1 × 10^{15} cm^{-2}, increasing from left to right. (*b*) Plan and cross-sectional views of similar SOPS waveguides fabricated using a large area irradiation fluence of 2 × 10^{13} cm^{-2}. (*c*) Left: the schematic diagram of the fabrication process of Bragg waveguides in silicon; right: the cross-sectional SEM image of Bragg cladding waveguide irradiated with a fluence of 2 × 10^{15} cm^{-2}. (*a*) Reprinted with permission from [59], (*b*) reprinted with permission from [58], Copyright 2009, Optical Society of America. (*c*) Reprinted with permission from [61]. Copyright 2010, Optical Society of America.

produced using direct writing [59]. A low surface roughness of 3 nm rms is achieved after subsequent oxidation, resulting in measured propagation losses of ∼1 dB cm^{-1}, the lowest reported loss for SOPS waveguides. Figure 10(*a*) shows three such waveguides formed with different proton fluences, where the oxide cladding is seen. The core size depends on the proton fluence, so consequently the propagation loss also depends on the fluence. A fluence of 10^{15} cm^{-2} produced the largest core and so the lowest loss, though not just because of the larger size but also because of the greater likelihood of a uniform irradiation at higher fluences.

The effect of oxidation on the propagation loss and surface roughness was also studied on similar waveguides fabricated using large area irradiation with 250 keV protons, figure 10(*b*) [60]. A thin thermal oxide is formed around the core of the waveguide, enabling the symmetric reduction of core size and roughness on all sides. Significant loss reduction from about 10 to 1 dB cm^{-1} is obtained after oxidation smoothening.

A single-mode Bragg cladding rib waveguide is also demonstrated in 0.02 W cm silicon [61], which consists of PSi layers with a low refractive index core that is bounded by DBRs comprising eight bilayers of alternating high and low refractive index. Irradiation acts to reduce the thickness of PSi formed, as described in section 3, creating an optical barrier needed for lateral confinement. Single mode guiding with losses as low as approximately 1 dB cm^{-1} was obtained over a broad range of wavelengths, offering a possible method for monolithic integration of Bragg waveguides in silicon, without multiple processes of depositing alternating materials.

5. Conclusions

We have demonstrated a range of micromachined structures which can be produced using various modes of irradiation based around the central principle of using ion irradiation as a means of locally varying and controlling the flow of a hole current during electrochemical anodization by introducing a defect profile which can be varied both in depth and laterally. This has enabled us to produce a range of two- and three-dimensional silicon microstructures for a variety of research fields.

Acknowledgments

We wish to thank Drs E J Teo, Dharmalingham Mangaiyarkarasi and Ow Yueh Sheng for their contributions to the work described in this review.

References

[1] Elwenspoek M and Jansen H V 2004 *Silicon Micromachining* (Cambridge: Cambridge University Press)
[2] Kelsall R, Hamley I W and Geoghegan M 2005 *Nanoscale Science and Technology* (New York: Wiley)
[3] Reed G T 2008 *Silicon Photonics: The State of the Art* (New York: Wiley)
[4] Allen J J 2005 *Micro Electro Mechanical System Design* (Boca Raton, FL: CRC Press)
[5] Li Y, Qian F, Xiang J and Lieber C M 2006 *Mater. Today* **9** 18
[6] Voldman J, Gray M L and Schmidt M A 1999 *Annu. Rev. Biomed. Eng.* **1** 401
[7] Bühler J, Steiner F P and Baltes H 1997 *J. Micromech. Microeng.* **7** R1
[8] Bustillo J M, Howe R T and Muller R S 1998 *Proc. IEEE* **86** 1552
[9] Luoto H, Henttinen K, Suni T, Dekker J, Mäkinen J and Torkkeli A 2007 *Solid-State Electron.* **51** 328
[10] Steve R and Robert P 2001 *J. Micromech. Microeng.* **11** 287
[11] Langford R M, Dale G, Hopkins P J, Ewen P J S and Petford-Long A K 2002 *J. Micromech. Microeng.* **12** 111
[12] Chekurov N, Grigoras K, Sainiemi L, Peltonen A, Tittonen I and Franssila S 2010 *J. Micromech. Microeng.* **20** 085009
[13] Henry M D, Shearn M J, Chhim B and Scherer A 2010 *Nanotechnology* **21** 245303
[14] Laermer F and Schilp A 1996 *US Patent* 5501893
[15] Ayon A A, Braff R, Lin C C, Sawin H H and Schmidt M A 1999 *J. Electrochem. Soc.* **146** 339
[16] Christopher M W, Alireza M and Reza G 2003 *J. Micromech. Microeng.* **13** 170
[17] Christophersen M and Phlips B F 2008 *Appl. Phys. Lett.* **92** 194102
[18] Azimi S, Sandoughsaz A, Amirsolaimani B, Naghsh-Nilchi J and Mohajerzadeh S 2011 *J. Micromech. Microeng.* **21** 074005

[19] Arne S and Helmut S 2010 *J. Micromech. Microeng.* **20** 095002

[20] Wang Y, Kanamori Y, Sasaki T and Hane K 2009 *J. Micromech. Microeng.* **19** 025019

[21] Breese M B H, Grime G W and Watt F 1992 *Annu. Rev. Nucl. Part. Sci.* **42** 1

[22] Breese M B H, Jamieson D N and King P J C 1996 *Materials Analysis Using a Nuclear Microprobe* (New York: Wiley)

[23] Watt F, Breese M B H, Bettiol A A and van Kan J A 2007 *Mater. Today* **10** 20

[24] Svensson B G, Mohadjeri B, Hallén A, Svensson J H and Corbett J W 1991 *Phys. Rev.* B **43** 2292

[25] Hallen A, Keskitalo N, Masszi F and Nagl V 1996 *J. Appl. Phys.* **79** 3906

[26] Ziegler J F, Ziegler M D and Biersack J P 2010 *Nucl. Instrum. Methods Phys. Res.* B **268** 1818

[27] Polesello P *et al* 1999 *Nucl. Instrum. Methods Phys. Res.* B **158** 173

[28] Rajta I, Szilasi S Z, Fürjes P, Fekete Z and Dücső C 2009 *Nucl. Instrum. Methods Phys. Res.* B **267** 2292

[29] Menzel F, Spemann D, Lenzner J, Böhlmann W, Zimmermann G and Butz T 2009 *Nucl. Instrum. Methods Phys. Res.* B **267** 2321

[30] Schulte-Borchers M, Vetter U, Koppe T and Hofsäss H 2012 *J. Micromech. Microeng.* **22** 025011

[31] Mangaiyarkarasi D, Sheng O Y, Breese M B, Fuh V L and Xioasong E T 2008 *Opt. Express* **16** 12757

[32] Mangaiyarkarasi D, Breese M B H, Ow Y S and Vijila C 2006 *Appl. Phys. Lett.* **89** 021910

[33] Berger M G, Arens-Fischer R, Thönissen M, Krüger M, Billat S, Lüth H, Hilbrich S, Theiß W and Grosse P 1997 *Thin Solid Films* **297** 237

[34] Pavesi L 1997 *Nuovo Cimento* **20** 1

[35] Vincent G 1994 *Appl. Phys. Lett.* **64** 2367

[36] Lehmann V 2002 *Electrochemistry of Silicon: Instrumentation, Science, Materials and Applications* (Weinheim, Germany: Wiley)

[37] Mangaiyarkarasi D, Breese M B H, Sheng O Y and Blackwood D J 2007 *Nucl. Instrum. Methods Phys. Rev.* B **260** 445

[38] Mangaiyarkarasi D, Breese M B H and Ow Y S 2008 *Appl. Phys. Lett.* **93** 221905

[39] Ow Y S, Azimi S, Breese M B H, Teo E J and Mangaiyarkarasi D 2010 *J. Vac. Sci. Technol.* B **28** 500

[40] Ow Y S, Breese M B H, Leng Y R, Azimi S, Teo E J and Sun X W 2010 *Nucl. Instrum. Methods Phys. Res.* B **268** 1416

[41] Ow Y S, Breese M B H and Azimi S 2010 *Opt. Express* **18** 14511

[42] Lai L and Irene E A 1999 *J. Appl. Phys.* **86** 1729

[43] Lee K K, Lim D R, Kimerling L C, Shin J and Cerrina F 2001 *Opt. Lett.* **26** 1888

[44] Wilson W L, Curtis K, Tackitt M, Hill A, Hale A, Schilling M, Boyd C, Campbell S, Dhar L and Harris A 2000 *Opt. Quantum Electron.* **32** 393

[45] Per G 2003 *Opt. Lasers Eng.* **40** 517

[46] Saari P, Kaarli R and Rätsep M 1993 *J. Lumin.* **56** 175

[47] Nishchal N K, Joseph J and Singh K 2004 *Opt. Eng.* **43** 2959

[48] Son J Y, Javidi B and Kwack K D 2006 *Proc. IEEE* **94** 502

[49] Azimi S, Ow Y S and Breese M B H 2010 *Electrochem. Solid-State Lett.* **13** H382

[50] Merenda F, Grossenbacher M, Jeney S, Forró L and Salathé R-P 2009 *Opt. Lett.* **34** 1063

[51] Merenda F, Rohner J, Fournier J-M and Salathé R-P 2007 *Opt. Express* **15** 6075

[52] Lin C-H, Wen S-Y and Hsu W 2004 *Japan Soc. Appl. Phys.* **43** 7764

[53] Aoki Y, Shimada Y and Iga K 2000 *IEEE Conf. on Lasers and Electro-Optics Europe: Conf. Digest.* p 1

[54] Jamois C, Wehrspohn R B, Andreani L C, Hermann C, Hess O and Gösele U 2003 *Photonics and Nanostructures—Fundamentals and Applications* (Amsterdam: Elsevier) vol 1 p 1

[55] Azimi S, Breese M B H, Dang Z Y, Yan Y, Ow Y S and Bettiol A A 2012 *J. Micromech. Microeng.* **22** 015015

[56] Breese M B H, Champeaux F J T, Teo E J, Bettiol A A and Blackwood D J 2006 *Phys. Rev.* B **73** 035428

[57] Ow Y S, Liang H D, Azimi S and Breese M B H 2011 *Electrochem. Solid-State Lett.* **14** D45

[58] Yang P Y, Mashanovich G Z, Gomez-Morilla I, Headley W R, Reed G T, Teo E J, Blackwood D J, Breese M B H and Bettiol A A 2007 *Appl. Phys. Lett.* **90** 241109

[59] Teo E J, Bettiol A A, Yang P, Breese M B H, Xiong B Q, Mashanovich G Z, Headley W R and Reed G T 2009 *Opt. Lett.* **34** 659

[60] Teo E J, Xiong B Q, Ow Y S, Breese M B H and Bettiol A A 2009 *Opt. Lett.* **34** 3142

[61] Teo E J, Bettiol A A, Xiong B, Breese M B H and Shuvan P T 2010 *Opt. Express* **18** 8816

[62] Breese M B H and Mangaiyarkarasi D 2007 *Opt. Express* **15** 5537–42